Journal of Alloys and Compounds 521 (2012) 126–133

Contents lists available at SciVerse ScienceDirect

Journal of Alloys and Compounds

journal homepage: www.elsevier.com/locate/jallcom

Field emission characteristics of carbon nanotube films fabricated on a metal mesh by filtration

J.S. Choi [a], H.S. Lee [a], J.C. Goak [a], Y. Seo [a], K.B. Kim [a], Y.H. Song [b], Y.C. Choi [c], N.S. Lee [a,*]

[a] Faculty of Nanotechnology and Advanced Materials Engineering, INAME & HMC, Sejong University, 98 Gunja-dong, Gwnagjin-gu, Seoul 143-747, South Korea
[b] Convergence Components and Material Research Lab., Electronics and Telecommunications Research Institute, Daejeon 305-700, South Korea
[c] Hanhwa Nanotechnology, 423-1 Chungchun-dong, BuPyung-gu, Incheon 403-030, South Korea

ARTICLE INFO

Article history:
Received 30 September 2011
Received in revised form 5 January 2012
Accepted 15 January 2012
Available online 28 January 2012

Keywords:
Field emission
Carbon nanotubes
Vacuum filtration
Metal mesh
Emission life span

ABSTRACT

A novel-structured field emitter was fabricated by vacuum-filtrating in sequence an aqueous suspension of thin, highly crystalline multiwalled carbon nanotubes (MWCNTs) and an aqueous suspension of thick, defective MWCNTs through a metal mesh placed on a polymer membrane. We could form a mechanically strong CNT film by weaving carbon nanotubes (CNTs) through the metal mesh residing inside the film. On drying at 70 °C, the polymer membrane was spontaneously separated from the CNT-mesh hybrid structure due to a large difference between their thermal expansion coefficients, producing vertically aligned bushes of thin CNTs on the CNT film. On top of the bushes, sharp CNT tips were well developed and worked excellently as field emitters. This structure was designed in such a way that the thin CNTs worked as field emitters while the thick CNTs supported the emitter CNTs. Our CNT emitters showed a high emission current density of 220 mA/cm^2 at 4.3 V/μm, and its emission life span, measured at 40 mA/cm^2 in a DC bias mode, was ~171 h. We expect that the CNT emitters with a novel structure are promising for the applications to field emission sources requiring small area but high current, for example, X-ray generators, microwave amplifiers, etc.

1. Introduction

Carbon nanotubes (CNTs) have drawn much attention as one of the superior materials for field emitters due to their high aspect ratios and nanometer scale in radii of curvature at tip and excellent electrical, mechanical, thermal, and chemical properties [1–3]. CNT emitters have been extensively explored not only for large area applications such as backlight units (BLUs) of liquid crystal displays (LCD) [4,5] and field emission lamps (FELs) [6,7] but also for small area but high current applications such as X-ray tubes [8–11] and microwave amplifiers [12,13]. For the latter applications, in particular, emission of high current from the small area CNT emitters may cause failure to them in a short period of time mainly due to Joule heating [14], field evaporation [15], or electrostatic interaction [16]. In order to solve such failure problems owing to high current field emission, CNT emitters should satisfy the requirements such as low electrical resistance, high crystallinity, optimum aspect ratio and distribution density, height uniformity, low outgassing rate, strong adhesion on substrates, etc. CNT emitters have been usually fabricated by vertical growth on substrates using chemical vapor deposition (CVD)[17], screen printing [18], spray coating [19], vacuum filtration [20], electrophoresis [21], and so on. Over the other methods, the vacuum filtration is of advantage since, in this method, we can choose CNTs having excellent electrical properties and crystallinity to prepare the CNT suspension and use a filtration membrane with a controlled pore size and morphology to optimize the aspect ratios, distribution density, and height uniformity of CNT emitters. This method, based on the solution processes, is simple and low cost. Furthermore, the filtration method is characteristic of low outgassing in vacuum during field emission because surfactants and solvent involved in the CNT suspension can be completely removed on annealing the filtrated CNT film.

Qian et al. [22] have reported that the CNT emitters prepared by vacuum filtration showed better field emission properties than those by screen printing for large area LCD-BLU applications. Although vacuum filtration is more appropriate for fabricating small area CNT emitters, there have been few studies on the application of vacuum filtration to fabrication of small area but high current CNT emitters. Thus, we investigate the fabrication of the CNT emitters by using vacuum filtration and their field emission characteristics for small area, high current applications. In this work, CNTs were filtrated through a metal mesh placed on a polymer membrane. A mechanically strong CNT film was designed to be formed by weaving CNTs through the metal mesh residing inside the film. Two types of CNT suspensions were filtrated in sequence:

* Corresponding author. Tel.: +82 2 3408 3786; fax: +82 2 3408 4342.
E-mail address: nslee@sejong.ac.kr (N.S. Lee).

0925-8388/$ – see front matter © 2012 Elsevier B.V. All rights reserved.
doi:10.1016/j.jallcom.2012.01.074

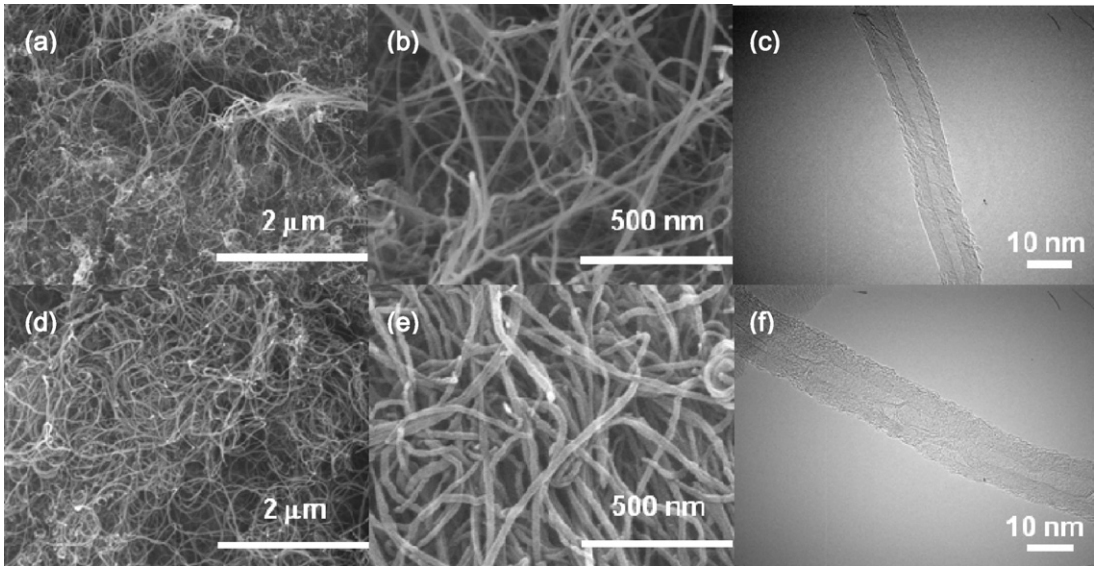

Fig. 1. SEM and TEM images of (a–c) thin and (d–f) thick CNTs used for emission and supporting layers, respectively. (c) and (f) are TEM images, and others are SEM images.

multi-walled CNTs (MWCNTs) with small diameters, short length, and high crystallinity and MWCNTs with large diameters, long length and low crystallinity. The former and latter CNTs were called as thin and thick CNTs, respectively. The thin CNTs formed an emission layer on the surface of the CNT film while the thick CNTs were strongly entangled with the metal mesh, forming a supporting layer of the emission layer. When the CNT film was separated by itself from the membrane during drying, the vertical CNT bushes were automatically developed with sharp tips on the film surface without further surface activation. In this report, we were able to fabricate small area but high current field emitters by incorporating the metal mesh, combining the two different types of CNTs, and optimizing the pore size of membrane.

2. Experimental

This study used thin and thick MWCNTs (Hanwha Nanotech Inc., Korea) as shown in Fig. 1. The CNTs were characterized by using Raman spectroscopy, thermogravimetric analysis (TGA), scanning electron microscopy (SEM), and transmission electron microscopy (TEM). CNTs featured the G peak at ~1582 cm^{-1} and the D peak at ~1350 cm^{-1}, which were attributed to stretching C-C bond and structural defects or impurities such as amorphous carbon, respectively [23]. In most cases, the crystallinity of CNTs is evaluated by the intensity ratio of G peak to D peak. In other way, the crystallinity of CNTs may be assessed by their oxidation

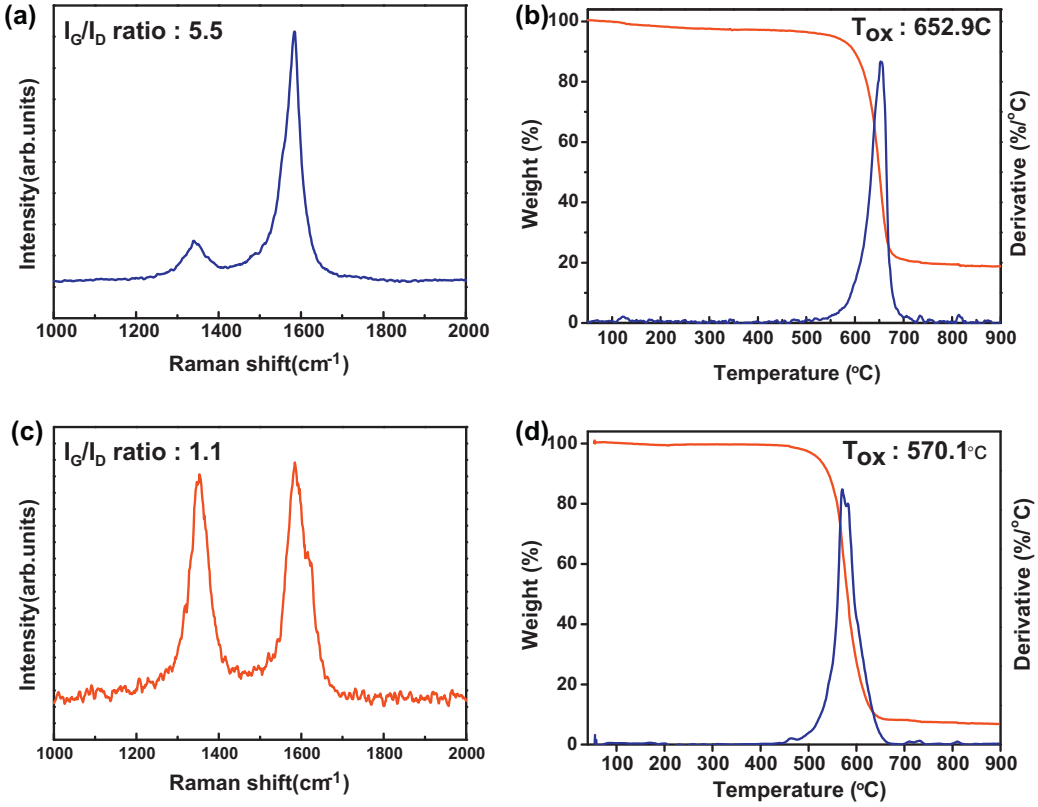

Fig. 2. Raman spectra and thermogravimetric analysis (TGA) and derivative thermogravimetric (DTG) curves (a, b) thin and (c, d) thick MWCNTs.

temperatures, peak temperatures in their differential thermogravimetric (DTG) curves. Non-carbonaceous impurities in pristine CNTs can be quantified by measuring a weight of residues remaining after burning up to 900 °C in TGA. The thin MWCNTs were of quite straight shape and excellent dispersibility in water. As seen in Fig. 1, the thin CNTs were 2–9 nm in diameter and 10–20 μm in length, measured by TEM and SEM, respectively. As given in Fig. 2, they were characteristic of the I_G/I_D ratio of 5.5, the oxidation temperature of 652.9 °C, and the non-carbonaceous impurities of 18.8 wt.%. The thick MWCNTs were entangled to form lumps. The thick CNTs were 12–17 nm in diameter, ~200 μm in length, 1.1 in I_G/I_D ratio, 570.1 °C in oxidation temperature, 6.9 wt.% in non-carbonaceous impurities. Comparing the thin and thick CNTs, the thin CNTs showed smaller diameters and shorter length, but higher crystallinity and thermal stability, known from their larger I_G/I_D ratio and higher oxidation temperature.

For each of the thin and thick CNTs, 100 mg CNTs were dispersed in 100 ml of distilled water containing 1 g of sodium dodecyl sulfate (SDS) with a horn-type sonicator (300 W) for 30 min. After centrifuging at 10,000 g for 15 min, the top 80% of the solution was obtained by using a pipette, producing the CNT dispersion with metal impurities and non-dispersed lumps removed. The yields of the thin and thick CNTs in the suspensions were measured to be ~56% and ~72%, respectively, assessed with optical absorptions at the wavelength of 700 nm.

CNT emitters were fabricated as schematically demonstrated in Fig. 3. First, a metal mesh was placed just on a polymer membrane. Second, the thin CNT suspension was vacuum-filtrated through the assembly of a metal mesh and a polymer membrane, third, followed by filtration of the thick CNT suspension. We used a polyvinylidene difluoride (PVDF) membrane with pores of 0.45 μm and mixed cellulose ester (MCE) membranes with pores of 1, 3, and 5 μm. The #500 metal (stainless 304) mesh had the opening area of 28 μm × 28 μm and the thickness of 60 μm. After filtrating each of the thin and thick CNT suspensions, we rinsed sufficiently the CNT film with plenty of distilled water to eliminate excessive SDS. Fourth, the CNT film was dried for 6 h at 70 °C. During the drying process, the polymer membrane would undergo large thermal expansion while the metal mesh would do little. Specifically, the thermal expansion coefficient of PVDF is about two orders of magnitude higher than that of SUS 304 [24,25]. The CNT film, interwoven with the metal mesh, would follow the behavior of the metal mesh on drying. A large difference in their thermal expansions between the metal mesh and the polymer membrane made the CNT-mesh hybrid structure delaminated from the membrane, causing sharp CNT emitter tips on the CNT film surface. The CNT film was fired in air at 350 °C to completely burn out residual SDS (our TGA experiment confirmed that SDS was completely removed at 300 °C in air). On the other hand, when the metal mesh was not engaged, the CNT film followed the thermal expansion of the membrane and thus was not separated during drying. In this case, the polymer membrane was removed by acetone, and the remaining CNT film was fired at 350 °C. Thereafter, CNT emitter tips were formed by surface activation with an adhesive tape [26] for the case where a metal mesh was not involved.

The CNT film was glued onto a stainless steel plate by using an Ag paste for field emission measurement. A tungsten anode plate was kept apart from a cathode plate with a 340 μm-thick alumina sheet spacer inserted in-between. An emission area of the cathode was 0.5 cm × 0.5 cm, and a vacuum level was maintained to be ~5×10^{-7} Torr. A dc voltage (HCN1400-12500, Fug) was biased to the anode while grounding the cathode. Field emission current (HP34401A, Agilent) was measured between the cathode and the ground. A life span of the CNT emitter sample was evaluated by measuring a length of time during which an initial current density of 40 mA/cm^2 was decreased to its half value.

3. Results and discussion

3.1. Metal mesh engaged inside CNT films

Fig. 4 shows SEM images of CNT films fabricated without and with a metal mesh engaged inside. Both CNT films were produced by filtrating in sequence 10 ml of the thin CNT suspension and 10 ml of the thick CNT suspension. With the same amounts of the CNT suspensions filtrated, two films show quite different thicknesses,

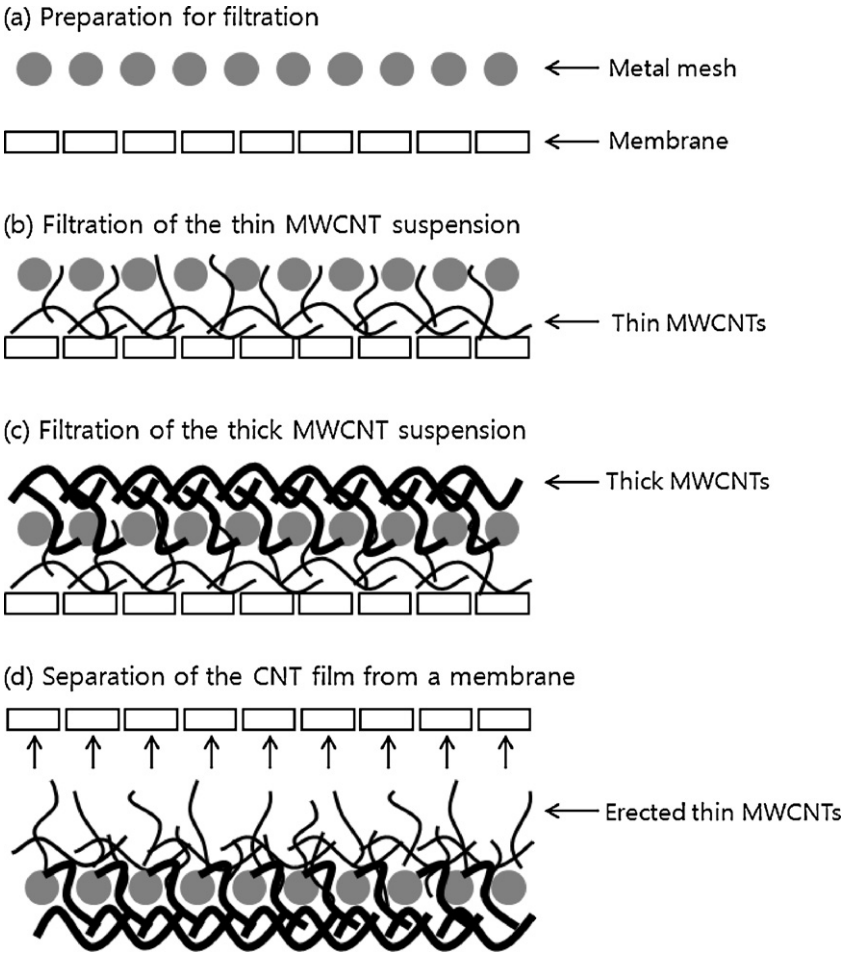

Fig. 3. Schematic of the fabrication procedures of CNT emitters: (a) preparation for filtration by placing a metal mesh on a polymer membrane, filtration of (b) the thin MWCNT suspension and (c) thick MWCNT suspension through the assembly of a metal mesh and a membrane, and (d) spontaneous separation of the CNT film from the polymer membrane during drying.

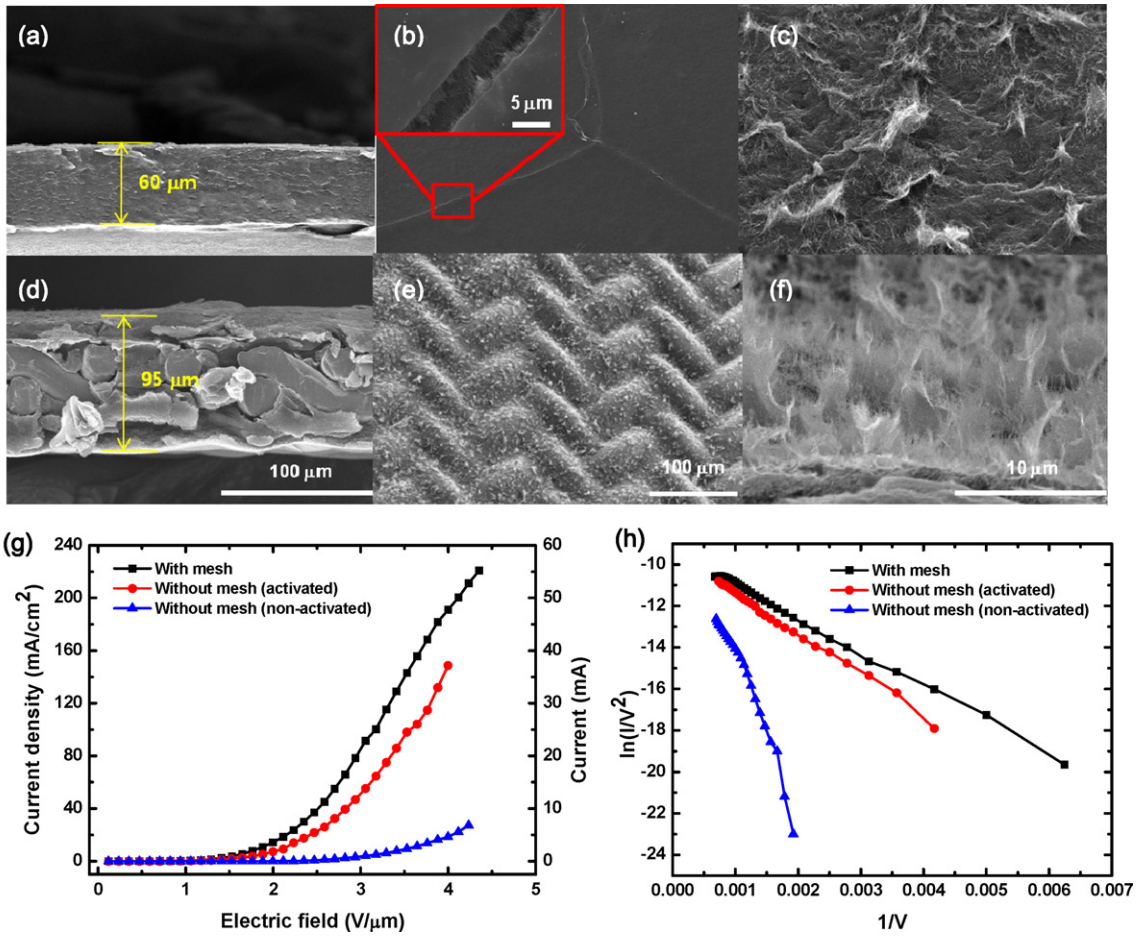

Fig. 4. (a, d) Cross-sectional, (b, e) planar, and (c, f) 60°-tilted (from the plane) SEM images of CNT films fabricated (a–c) without and (d–f) with a metal mesh, (g) their field emission current density–electric field curves, and (h) their corresponding Fowler–Nordheim plots. All samples are subjected to firing, and images (a–c) are observed after tape activation.

according to the incorporation of the mesh. Without a mesh, a dense CNT film occurred with the thickness of 60 μm due to strong contraction by firing, as given in Fig. 4(a). On incorporating a mesh, however, the thickness of the CNT film increased to 95 μm because the 60 μm-thick metal mesh was inserted in the middle of the CNT film. The CNT films showed different surface morphologies depending on whether a metal mesh was placed or not. Without a mesh, cracks occurred on the CNT film surface probably due to contraction during firing, indicating that the CNT film was quite fragile, as shown in Fig. 4(b). An inset shows a high-magnification SEM image on the surface crack formed in the designated area of the CNT film without a mesh. In contrast, the CNT-mesh hybrid film, where a mesh was embedded inside, showed rigid mechanical integrity and thus was not accompanied with occurrence of cracks on the surface. The CNT film without a mesh exhibited a flat surface because it was of uniform contraction along a thickness direction on firing. On the other hand, the CNT film with a mesh showed a surface which was corrugated in a zigzag fashion following the wire frame structure of the underlying mesh, as presented in Fig. 4(e), because the film was contracted more in the openings than in the wires of the mesh. Thus, depressions occurred in the openings while and protrusions took place in the wires of the mesh. Since the surface was flat for the film without a mesh, the surface was activated by peeling off its epidermal layer with an adhesive tape so that CNTs could be vertically erected on the surface and could work as field emitters. As seen in Fig. 4(c), however, the tape activation could not easily make CNTs stand up on the surface because the CNT film was too tightly consolidated. For the CNT film with a metal mesh, on the contrary, many CNTs were erected upward without tape activation. The CNT film was separated by itself from the polymer membrane due to a large difference in thermal expansions between the polymer and the CNT-mesh hybrid structure during drying at 70 °C. CNTs were sucked into the membrane pores during filtration, and the epidermal CNT layer stuck onto the membrane was torn off from the main CNT-mesh hybrid film during drying. On separation, CNT bushes were developed on the CNT-mesh hybrid film. Closely looking at the bushes, CNTs were vertically aligned without additional activation and were expected to work as excellent field emitters, as shown in Fig. 4(f).

Field emission current density (J) versus electric field (E) curves, measured from the CNT film without and with a metal mesh, are given in Fig. 4(g). For the CNT film without a mesh, the J–E curves were measured before and after surface activation with a tape. The CNT film without a mesh showed turn-on electric fields (E_{to}) of 1.76, and 0.71 before and after activation, respectively. E_{to} is defined as an E where an emission current of 1 μA is recorded. With a mesh inserted, E_{to} was lowered 0.59 V/μm. At an E of 4 V/μm, the CNT film without a mesh exhibited J of 18.5 and 148.6 mA/cm^2 before and after activation, respectively, while the CNT film with a mesh showed a much higher J of 190.9 mA/cm^2 at the same E. Such excellent field emission characteristics of the CNT film with a mesh seemed to be attributed to the development of CNT bushes with vertically aligned CNT tips.

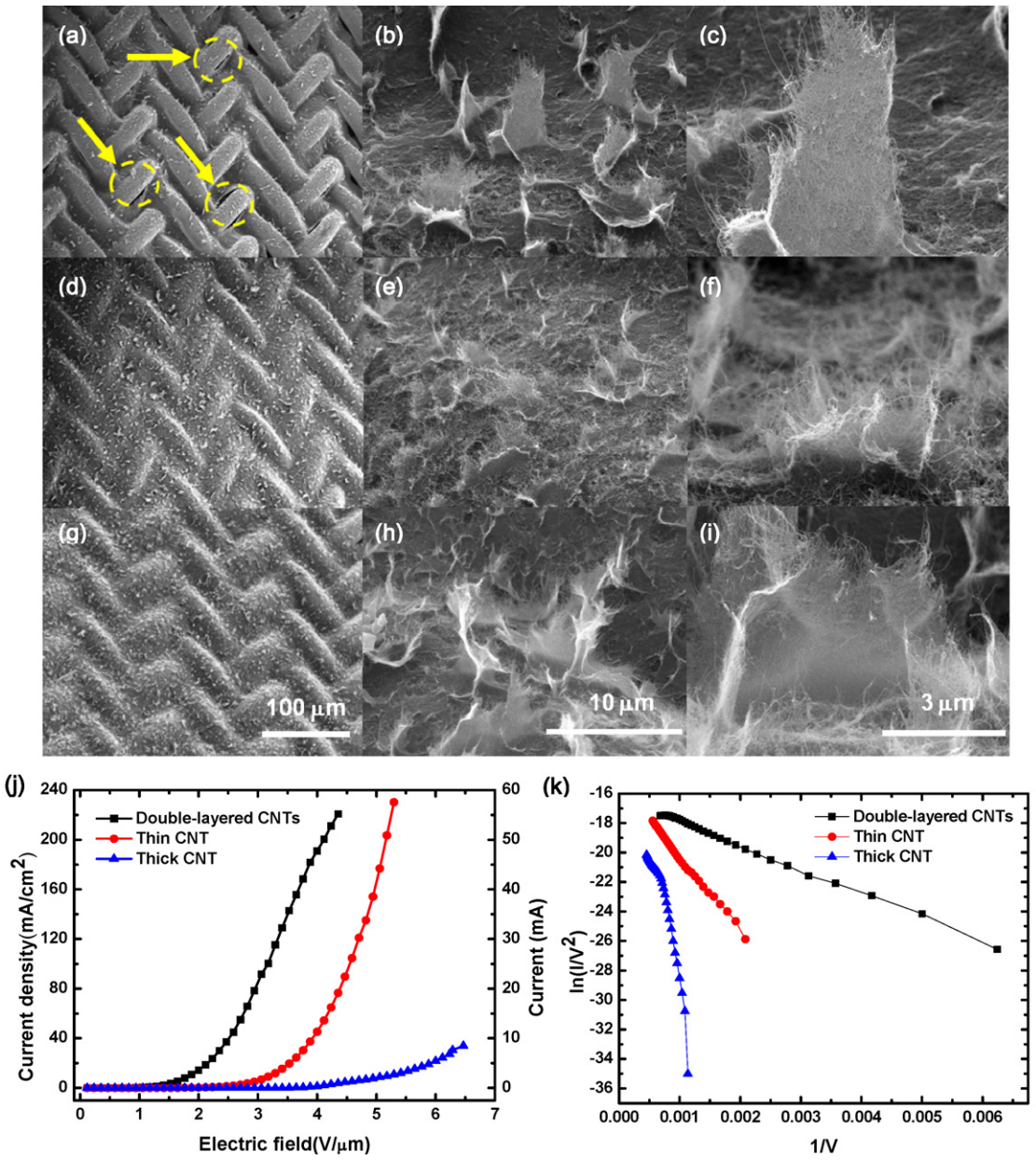

Fig. 5. 45°-tilted SEM images of the CNT films fabricated (a–c) only with thin CNTs, (d–f) only with thick CNTs, (g–i) with both thin and thick CNTs, (j) their field emission *J–E* curves, and (k) their corresponding Fowler–Nordheim plots.

Fig. 4(h) shows Fowler–Nordheim (F–N) plots, obtained from the corresponding *J–E* curves by using the F–N equation [27],

$$\ln\left(\frac{I}{V^2}\right) = \ln\left(A\alpha\phi^{-1}\frac{\beta^2}{d^2}\right) - \frac{B\phi^{3/2}d}{\beta}\left(\frac{1}{V}\right)$$

Here, an emission current I can be related to an applied voltage V, depending on an effective emission area α, a field enhancement factor β, a work function of an emitter Ø, and a cathode-to-anode distance d. A and B are constant, 1.54×10^{-6} A eV V^{-2} and 6.83×10^{7} eV$^{-3/2}$ V cm^{-1}, respectively. The F–N plots show a linear inverse relationship between a logarithmic value of I/V^2 and $1/V$. Assuming Ø, of 4.61 eV for CNTs [28], the β values of the CNT film without a mesh before and after activation were computed to be 2638 and 10,306, respectively. The tape activation greatly improved field emission characteristics of the CNT film without a mesh. An introduction of a mesh into a CNT film enhanced further the β value to 12,351. The β value is governed only by a geometrical shape of an emitter for a given Ø, indicating how many times an applied external E (V/d) is enhanced locally at an emitter tip. The longer the CNT emitters (assuming their diameters to be constant) are, the larger the β values are. These results are well consistent with our SEM observations of Fig. 4(c) and (f).

3.2. CNT films fabricated by using thin and thick CNTs

We prepared the CNT films by vacuum-filtrating the solutions of thin and thick CNTs through the assembly of a metal mesh and a polymer membrane. Fig. 5(a)–(c) shows the CNT film fabricated by using only the thin CNT solution. This CNT film was largely contracted during firing, as seen in Fig. 5(a), probably because thin CNTs were of small diameters and short length. Such a large contraction caused a wavy surface well developed following the wire frame structure of the mesh underlying the CNT film and also gave rise to cracks on some borders between depressed and protruded

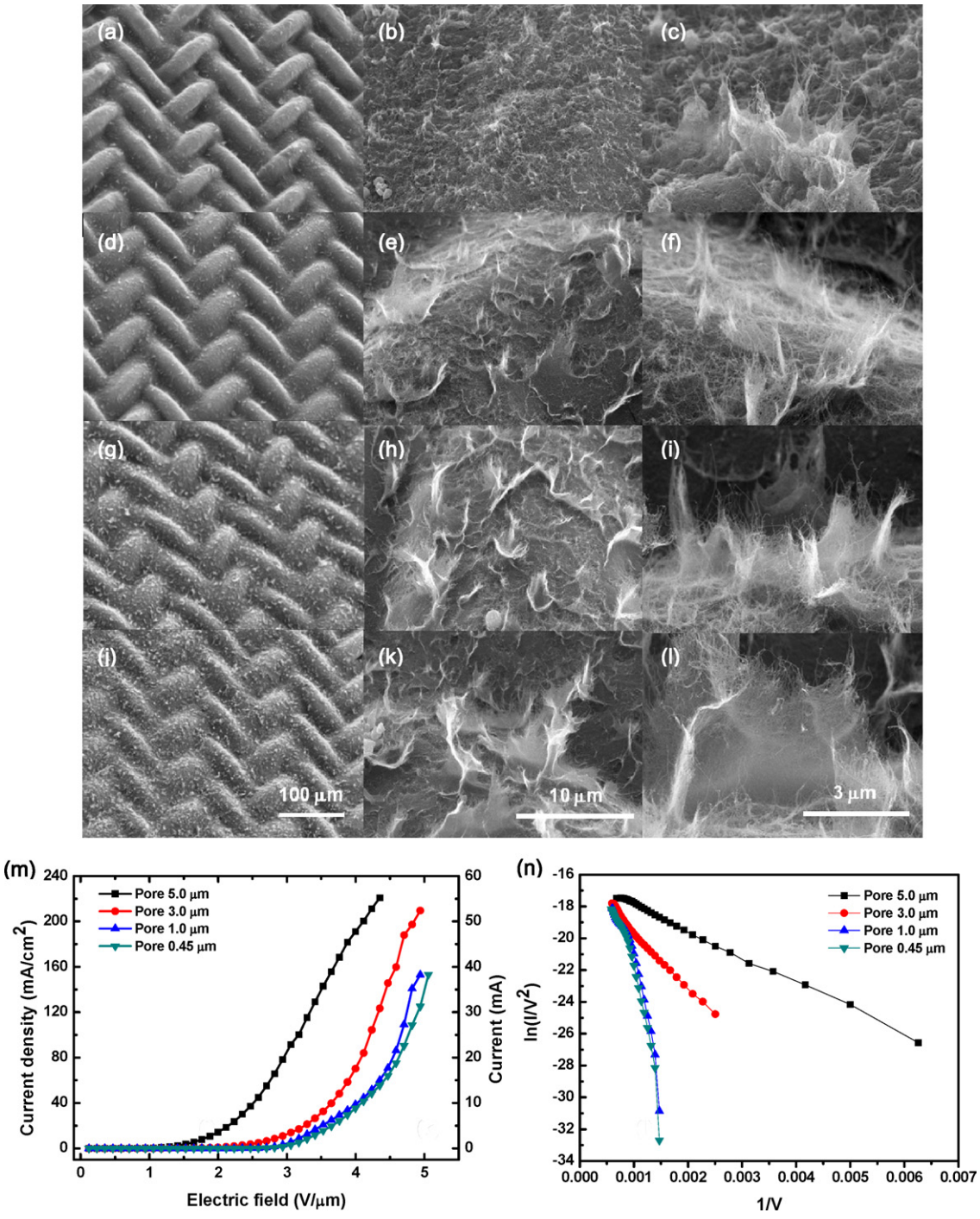

Fig. 6. 45°-tilted SEM images of the CNT films fabricated with polymer membranes with different pore sizes of (a–c) 0.45, (d–f) 1, (g–i) 3, and (j–l) 5 μm, (m) their field emission *J–E* curves, and (n) their corresponding Fowler–Nordheim plots.

regions, as indicated by dotted circles in Fig. 5(a). As thin CNTs were deeply sucked into the membrane pores during vacuum filtration, CNT bushes seemed to be developed with high elevations on separation, as seen in Fig. 5(b) and (c). Closely looking at the tips of these bushes, CNTs stuck out in spikes and were expected to work as excellent field emitters. On the other hand, the CNT film made of thick CNTs were less contracted and thus were less corrugated on the surface, as given in Fig. 5(d), since thick CNTs seemed to form strong networks in the film probably due to their thick diameters, large length, and entangled character. Thick CNTs were less sucked into the membrane pores, resulting in the development of CNT bushes with short lengths. The film of thin CNTs showed well-developed, tall bushes while that of thick CNTs was flatter on the surface. Since the film made of either thin or thick solution showed both pros and cons, this study intended to strengthen its strengths and make up for its weaknesses by filtrating each of the suspensions of thin and thick CNTs in sequence through the mesh-membrane assembly. In the double-layered CNT film involving two types of CNTs, thin CNTs would play their roles as field emitters by building tall, spiky CNT bushes on the surface, and thick CNTs would work as supporters for the emission CNT layer by forming strong networks underneath it through a metal mesh. Fig. 5(g)–(i) shows the CNT film whose top surface and underlying layers were made of thin and thick CNTs, respectively. As a result, its surface

corrugation was formed in the middle between the above two films made of only either thin or thick CNTs, and cracks did not occur. The double-layered CNT film showed CNT bushes similar to those of the film of thin CNTs in morphology.

Fig. 5(j) presents field emission *J*–*E* curves of the CNT films fabricated by using thin, thick, or both CNTs. Only with thick CNTs, E_{to} was 3.06 V/μm. By using only thin CNTs, E_{to} was lowered to 1.29 V/μm. For the double-layered film using both thin and thick CNTs, E_{to} was further decreased to 0.59 V/μm. Their β values were 1171, 4006 and 12,351, respectively, calculated from their corresponding F–N plots given in Fig. 5(k). The thin-CNT film showed a lower E_{to} and higher β value than the thick-CNT film because CNT bushes were not only higher in elevation but spiky CNTs on the bushes were also smaller in diameter. The double-layered CNT film was expected to exhibit field emission properties similar to those of the thin-CNT film as the bushes were made of thin CNTs for both films. However, the double-layered CNT film showed a far lower E_{to} and higher β value than expected probably because the double-layered film had a much flatter surface than the thin-CNT film did, as can be compared in Fig. 5(a) and (g). In Fig. 5(a), electron emission would occur only from the protruded regions formed on the wire ridges of the mesh. Since the double-layered CNT film was less corrugated on the surface, a larger number of CNTs from wider hill areas would participate in field emission. Improvement of field emission characteristics of the double-layered CNT film seemed to be attributed to a decrease of surface corrugation.

3.3. CNT films fabricated with polymer membranes with different pore sizes

When each of the thin and thick CNT solutions was filtrated in sequence through the membrane-mesh assembly, we used polymer membranes with different pore sizes. Fig. 6 shows the double-layered CNT films fabricated by varying the pore size from 0.45 μm to 1, 3, and 5 μm. Observing the first-column images of Fig. 6, the CNT film surface is less corrugated with a larger pore size. As the pore size of the membrane increases, the vacuum filtration would create a greater suction force through the CNT-mesh hybrid film. The film, which becomes more compacted with increasing the pore size, is less contracted upon drying and finally less corrugated on the surface. As seen in the first-column images of Fig. 6, the surface becomes flatter with a larger pore size, resulting in a larger emission area for the film fabricated on the membrane with an increasing pore size. The second and third columns of Fig. 6 show that the CNT bushes are developed taller with a larger pore size. When the CNT film was separated by itself from the membrane while drying, the epidermal CNT layer with the part of it suck into the membrane was torn off from the main CNT-mesh hybrid film. A larger amount of CNTs would be sucked more deeply into the pores with a larger size during vacuum filtration. Thus, the CNT bushes, which were formed by tearing of the CNT film, would be developed taller as increasing the pore size.

Field emission *J*–*E* curves and their F–N plots as a function of a pore size are presented in Fig. 6(m) and (n). The E_{to} values were 2.33, 2.11, 1.17, and 0.59 V/μm, and the β values were 1748, 1925, 5457, and 12,351 for the pore sizes of 0.45, 1, 3, and 5 μm, respectively. E_{to} was decreased while β was increased with a larger pore size. Improvement of field emission characteristics with increasing a pore size seems to be attributed to formation of taller CNT bushes and a larger emission area on the surface.

3.4. Measurement of field emission life span of CNT emitters

Fig. 7 demonstrates a field emission life span of the double-layered CNT film fabricated by using the membrane pore size of 5 μm and a metal mesh. Life span is defined as a period of time

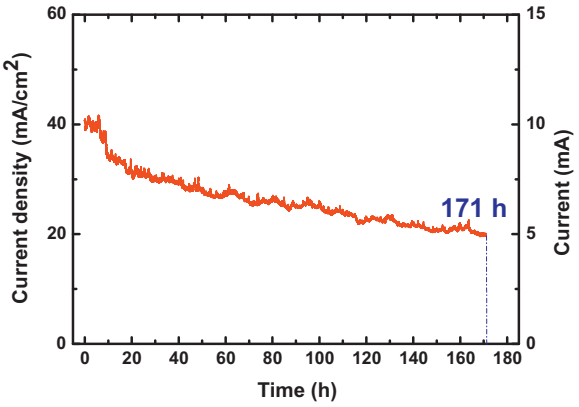

Fig. 7. Field emission lifespan curve of the CNT film fabricated with the membrane pore size of 5 μm, measured under a constant DC voltage.

taken for *J* to drop to half its initial value while applying a constant *E*. It took ~171 h to reach from an initial current density of 40 mA/cm^2 to its half value. Emission current was gradually lowered in a decreasing manner with time. The double-layered CNT film prepared by using a metal mesh and a membrane with a pore size of 5 μm shows quite a long field emission life span under a high current emission.

4. Conclusions

To apply to field emitters with a capability of high current emission, a CNT film was fabricated by filtrating aqueous CNT suspensions through a metal mesh placed on a polymer membrane. A metal mesh was imbedded inside the CNT film, expectedly providing a rigid CNT-mesh hybrid film. CNT bushes, standing upright and having individual CNTs at tip, were voluntarily developed on the film surface when the epidermal CNT layer stuck onto the membrane was torn off from the CNT-mesh hybrid film by itself while drying. The double-layered CNT film was prepared by filtrating each of the aqueous suspensions of thin and thick CNTs in sequence, where the thin CNTs worked as field emitters on the surface while the thick CNTs were interwoven with a metal mesh and formed a supporting layer underneath the emission layer. Field emission characteristics were improved by increasing the pore sizes of the membranes used in filtration as CNT bushes were developed taller with larger pore sizes. The double-layered CNT film, fabricated by using a metal mesh and a membrane of 5 μm-sized pores, exhibited a high emission current density of 220 mA/cm^2 at 4.3 V/μm, and a long emission life span, measured at 40 mA/cm^2 in a DC bias mode, of ~171 h. Our CNT films with a novel structure seem to be promising for the applications to field emitters producing high currents in small areas.

Acknowledgments

This work was supported by the Industrial Core Technology Development Program (no. 10037379) and by the Energy Efficiency & Resources of the Korea Institute of Energy Technology Evaluation and Planning grant (no. 2011201010090), both funded by the Ministry of Knowledge Economy, Korea.

References

[1] W.A. de Heer, A. Chatelaine, D. Ugarte, Science 270 (1995) 1179–1180.
[2] J.M. Bonard, J.P. Salvetat, T. Stöckli, L. Forró, A. Châtelain, Appl. Phys. A 69 (1999) 245–254.
[3] L.A. Chernozatonskii, Y.V. Gulyaev, Z.J. Kosakovskaja, N.I. Sinitsyn, G.V. Torgashov, F. Yu, Zakharchenko, E.A. Fedorov, V.P. Val′chuk, Chem. Phys. Lett. 233 (1995) 63–68.

[4] Y.C. Kim, E.H. Yoo, Jpn. J. Appl. Phys. 44 (2005) 454–456.
[5] Y.C. Choi, J.W. Lee, S.K. Lee, M.S. Kang, C.S. Lee, K.W. Jung, Nanotechnology 19 (2008) 235306–235310.
[6] D.J. Lee, S.I. Moon, Y.H. Lee, J.E. Yoo, J.H. Park, J. Jang, Vacuum 74 (2004) 105–111.
[7] Y.J. Jung, G.H. Son, J.H. Park, Y.W. Kim, Alexander S. Berdinsky, J.B. Yoo, C.Y. Park, Diamond Relat. Mater. 14 (2005) 2109–2112.
[8] G. Cao, Y.Z. Lee, R. Peng, Z. Liu, R. Rajaram, X. Calderon Colon, Phys. Med. Biol. 54 (2009) 2323–2340.
[9] G. Yang, R. Rajaram, G. Cao, S. Sultana, Z. Liu, D. Lalush, J. Lu, O. Zhou, Proc. SPIE 6913 (2008), pp. 1A1–1A10.
[10] Y. Sakai, A. Haga, S. Sugita, S. Kita, S.I. Tanaka, F. Okuyama, N. Kobayashi, Rev. Sci. Instrum. 78 (2007) 013305–013310.
[11] S.H. Heo, A. Ihsan, S.H. Yoo, G. Ali, S.O. Cho, Nanoscale Res. Lett. 5 (2010) 720–724.
[12] W.I. Milne, K.B.K. Teo, E. Minoux, O. Groening, J. Vac. Sci. Technol. B 24 (2006) 345–348.
[13] A.W. Scott, Understanding Microwaves, John Wiley & Sons, New York, 1993.
[14] J.M. Bonard, C. Klinke, K.A. Dean, B.F. Coll, Phys. Rev. B 67 (2003) 115406–115415.
[15] K.A. Dean, T.P. Burgin, B.R. Chalamala, Appl. Phys. Lett. 79 (2001) 1873–1875.
[16] A. Maiti, J. Andzelm, N. Tanpipat, P. Allmen, Phys. Rev. Lett. 87 (2001) 155502–155505.
[17] M. Sveningsson, R.E. Morjan, O.A. Nerushev, Y. Sato, J. Backstrom, E.E.B. Campbell, F. Rohmund, Appl. Phys. A 73 (2001) 409–418.
[18] J. Li, W. Lei, X. Zhang, X. Zhou, Q. Wang, Y. Zhang, B. Wang, Appl. Surf. Sci. 220 (2003) 96–104.
[19] E.S. Jang, J.C. Goak, H.S. Lee, S.H. Lee, J.H. Han, C.S. Lee, J.H. Sok, Y.H. Seo, K.S. Park, N.S. Lee, Appl. Surf. Sci. 256 (2010) 6838–6842.
[20] B.A. Kakade, V.K. Pillai, D.J. Late, P.G. Chavan, F.J. Sheini, M.A. More, D.S. Joag, Appl. Phys. Lett. 97 (2010) 073102–073104.
[21] B. Gao, G.Z. Yue, Q. Qiu, Y. Cheng, H. Shimoda, L. Fleming, O. Zhou, Adv. Mater. 13 (2001) 1770–1773.
[22] M. Qian, T. Feng, K. Wang, H. Ding, Y. Chen, Z. Sun, Appl. Surf. Sci. 256 (2010) 4642–4646.
[23] H.B. Zhang, G.D. Lin, Z.H. Zhou, X. Dong, T. Chen, Carbon 40 (2002) 2429–2436.
[24] Y. Xu, G. Ray, B. Abdel-Magid, Compos. Part. A: Appl. Sci. Manuf. 37 (2006) 114–121.
[25] J.S. Park, T.W. Kim, D. Stryakhiev, J.S. Lee, S.G. An, Y.S. Pyo, D.B. Lee, Y.G. Mo, D.U. Jin, H.K. Chung, Appl. Phys. Lett. 95 (2009) 013503–013505.
[26] T.J. Vink, M. Gillies, J.C. Kriege, H.W.J.J. van de Laar, Appl. Phys. Lett. 83 (2003) 3552–3554.
[27] R.G. Forbes, J. Vac. Sci. Technol. B 17 (1999) 526–533.
[28] C.J. Edgcombe, N. de Jonge, J. Phys. D: Appl. Phys. 40 (2007) 4123–4128.